ACS Photonics

pubs.acs.org/journal/apchd5

Article

Self-Configuring and Reconfigurable Silicon Photonic Signal Processor

Hailong Zhou,[§] Yuhe Zhao,[§] Xu Wang, Dingshan Gao, Jianji Dong,[*] and Xinliang Zhang

Cite This: *ACS Photonics* 2020, 7, 792−799

Read Online

ACCESS | Metrics & More | Article Recommendations | Supporting Information

ABSTRACT: Photonic signal processing is essential in the optical communication and optical computing. Numerous photonic signal processors have been proposed, but most of them exhibit limited reconfigurability and automaticity. A feature of fully automatic implementation and intelligent response is highly desirable for the multipurpose photonic signal processors. Here, a self-configuring and fully reconfigurable silicon photonic signal processor is proposed and experimentally demonstrated. The proposed photonic signal processor is capable of performing various functions, including multichannel optical switching, optical multiple-input-multiple-output descrambler, and tunable optical filter. All the functions are achieved by complete self-configuration without knowing the inner structure. Our demonstration suggests great potential for chip-scale fully programmable optical signal processing with the self-configuring ability.

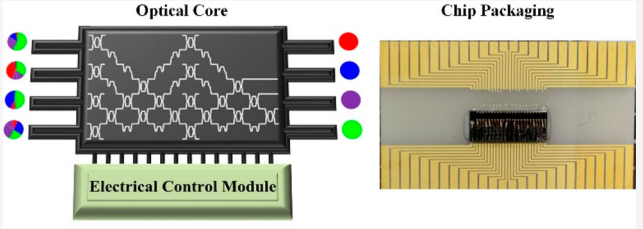

KEYWORDS: *silicon photonics, optical signal processing, gradient descent algorithm, programmable photonics*

Photonic signal processing is widespread both in the optical communication and optical computing. Almost all aspects of signal processing functions were developed, such as multichannel optical switching,[1−7] mode (de)multiplexer,[8,9] optical filter,[10−14] polarization management,[15−17] waveguide crossing,[18,19] and logic gates.[20−22] Plentiful photonic signal processing devices have been reported based on either discrete components or photonic integrated circuits.[1,9,15,20−24] Photonic signal processing devices based on discrete components are usually bulkier and less power efficient, whereas a photonic integrated signal processing chip has a much smaller footprint and a higher power efficiency. To date, various separated functional devices may make the system complex and high-cost. An effective solution is to implement low-cost and multipurpose signal processing in an optical network with a reconfigurable and integrated photonic signal processor. For example, a fully reconfigurable photonic integrated signal processor performed numerous types of optical computing based on an InP−InGaAsP material system.[25] Multipurpose silicon photonic signal processors were reported based on hexagonal waveguide mesh.[13,26,27] Silicon photonic polarization processor,[28] matrix computing processor,[29,30] tunable filters,[10−14] and programmable nanophotonic quantum processors[31−37] were also addressed. For these reconfigurable processors, a big challenge is how to dynamically configure these functions for reconfigurable photonic signal processors.

Most of the reported photonic signal processors were configured by manual operation.[1,2,12,14,25,27,38] It is cumbersome, time-consuming, and becomes extremely difficult when the network is expanded to a larger scale. Alternatively, some self-configuring methods were proposed. For example, the multipurpose processors could be trained using the feedback from the built-in optical power monitors,[39−42] whereas the internal monitors will introduce additional loss and the number of monitors will increase rapidly with the expansion of network, making both the electronic circuit and iterative algorithm quite complex. Besides, the inner structure of chips should be revealed in advance to the operators before any configuration of the system. The network could be alternatively trained by precalibration and subsequently analytic calculation of phase in each phase shifter.[13,26,27,43] However, it strongly depends on both the fabrication tolerance of chip network and the detailed information on the chip inner structure. It will be greatly complicated and difficult when the network is expanded to a larger one, since too much inner information is involved. Therefore, a fully automatic implementation of reconfigurable photonic signal processors capable of full self-configuration without knowing the detailed information on chip inner structure is highly required. That means only the input/output signals can be used for feedback, and the chip should self-learn to find the optimal solution starting from infancy.

In this paper, we report an intelligent photonic signal processor, which can perform three typical functions, including multichannel optical switching, optical multiple-input-multiple-output (MIMO) descrambler and tunable optical filter. All the

Received: November 25, 2019
Published: February 5, 2020

https://dx.doi.org/10.1021/acsphotonics.9b01673
ACS Photonics 2020, 7, 792−799

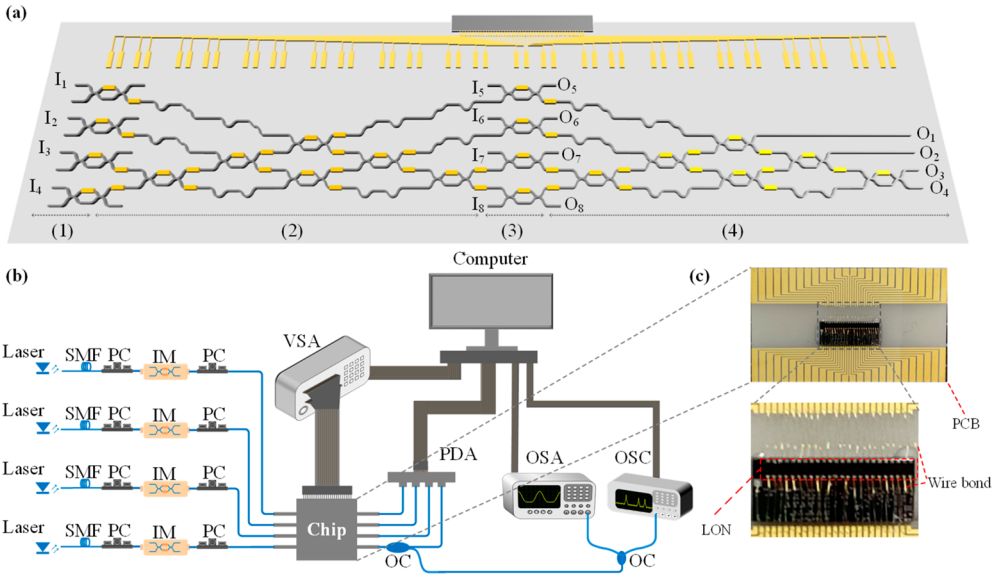

Figure 1. Optical signal processing circuits and schematic of the experimental setup. (a) The detailed structure of chip. (b) Schematic of the experimental setup. (c) The details of chip packaging. SMF: single mode fiber; PC, polarization controller; IM, intensity modulator; VSA, voltage source array; PDA, photodetector array; OC, optical coupler; OSA, optical spectrum analyzer; OSC, optical oscilloscope; LON, linear optical network; PCB, printed circuit board.

functions are programmable by self-configuration without any information about the inner structure. The training is accomplished using the numerical gradient descent algorithm modified from deep learning,[44,45] which is applicable for a general "black box" system. This demonstration is an important step toward the implementation of a multifunctional optical signal processor with the self-configuring ability.

PRINCIPLE AND EXPERIMENTAL SETUP

The photonic signal processor, structured with a silicon-based linear optical network (LON) shown in Figure 1a,[44,46,47] is fabricated on the commercial silicon-on-insulator (SOI) wafer (Supporting Information, section 1). The chip consists of four parts. Part (1) is constitutive of four Mach−Zehnder interferometers (MZIs), which are only in the "open" or "closed" state to switch the input channels. Parts (2) and (4) can both perform an arbitrary unitary matrix transformation (Supporting Information, section 2). Part (3) can perform an arbitrary diagonal matrix transformation or be used to switch the input channels, as same as Part (1). Parts (2), (3), and (4), as a whole, are used to implement an arbitrary matrix transformation based on singular value decomposition.[44,46] The chip contains 48 phase shifters and 20 MZIs totally. The experimental setup is depicted in Figure 1b. Four independent 10 Gbit/s nonreturn-to-zero (NRZ) signals are loaded into four laser beams at 1550 nm with the optical intensity modulators (IMs), and then the beams are launched into our chip through a V-groove fiber array (VGA). The polarizations of input/output light are optimized by inline polarization controllers (PCs). Another VGA and a 4-channel photodetector array (PDA) are used to receive the output light from the chip. Part of beams in a specified channel are separated by fiber optic couplers (OCs) and then fed into an optical spectrum analyzer (OSA) or an optical oscilloscope (OSC) for further analysis. All the phase shifters in the chip are driven by a voltage source array (VSA). All the monitoring instruments and voltage sources are connected and controlled by the same computer. Figure 1c shows the details of chip packaging. The SOI chip is glued on a ceramic-wafer printed circuit and the pads are wire-bonded to the printed circuit board (PCB). Based on this setup, multiple photonic signal processing functions can be implemented by self-configuration. According to the different purposes of signal processors, a suitable and special cost function (CF) should be first defined for a successful training (Supporting Information, section 3). Then the only training target is to make the defined CF maximum using the numerical gradient descent algorithm. In the following, the chip is reconfigured to achieve three different functions.

RESULTS

Multichannel Optical Switching. An n-channel optical switching is a standard matrix transformation given by (referred to in the Supporting Information, section 3)

$$M = [M_1 \quad M_2 \quad \ldots \quad M_n] \tag{1}$$

where M_1, M_2, ..., M_n are the realignment of standard unit vectors in n dimensional Hilbert space. M_j is the jth column vector of M, representing the power distribution at all the output ports when only the input Port j is switched on. The traditional optical link switching was accomplished by manual adjustment or semiautomaticity,[1,5,7] here we exploit the self-configuring method to implement the optical link switching automatically. In order to implement the optical switching irrelevant to the input powers, we define the CF as the correlation of experimental and theoretical vectors (see Supporting Information, section 3)

$$\mathrm{CF} = \prod_{j=1}^{n} \mathrm{Corr}(M_j, M\ \mathrm{exp}_j) \tag{2}$$

Here, $M\ \mathrm{exp}_j$ is the measured power distribution at all the output ports when only the input Port j is switched on. It can be accomplished by switching the input channel one by one with the MZIs in the front end of chip. The CF ranges from 0 to 1, where CF = 0 represents that the experimental results are

https://dx.doi.org/10.1021/acsphotonics.9b01673
ACS Photonics 2020, 7, 792−799

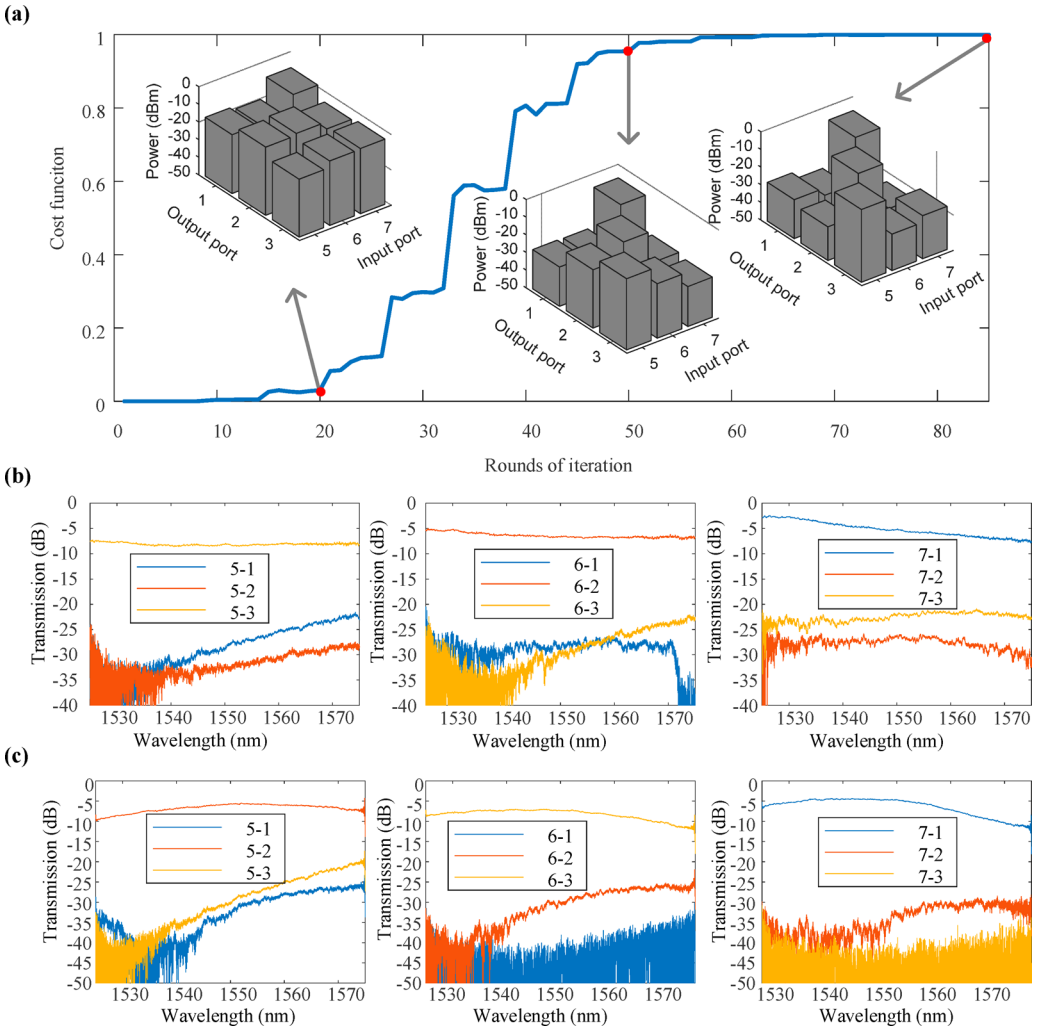

Figure 2. Multichannel optical switching. (a) Cost function dependent on the rounds of iteration in training process. The insets figures show the light power distributions when the round of iteration equals 20, 50, and 85, respectively. (b) Transmission spectra for the signal and noise of the optical links in the shown routing state: I_5-O_3, I_6-O_2, I_7-O_1. (c) Transmission spectra for the signal and noise of the optical links in the shown routing state: I_5-O_2, I_6-O_3, I_7-O_1. Also, see the Supporting Information of Video S1.

completely inconsistent to the targeted results and CF = 1 represents that they are completely consistent. Our training target is to make the CF close to 1 as much as possible. The training is accomplished using a modified gradient descent algorithm,[44] which is a universal method for training computational neural networks.[48−50] The detailed training algorithm is presented in Supporting Information, section 3. In our design, the matrix transformation of M can be implemented by Part (2) or Part (4). Thus, Part (1) and Part (2) are disabled. We use Part (4) to train the matrix and Part (3) to switch the input channels. The light is injected into input ports of I_5-I_8 and then output from O_1-O_4. Considering that only three input ports (I_5, I_6, I_7) can match the VGA (the gap of fibers is 127 um), only three-port matrix switches (I_5, I_6, I_7, O_1, O_2, and O_3) are used to carry out the proof-of-concept experiments.

To show the reconfigurability and self-configuring ability of our chip, we implement multiple routing states for the multichannel optical switching. Figure 2a presents the trainning process dependent on rounds of iteration in the routing state: I_5-O_3, I_6-O_2, I_7-O_1 (the iteration evolution is recorded by Video S1). In the beginning, the light power distributions for all output ports are random and messy. And strong crosstalk exists between these channels. The first inset of Figure 2a shows an example of power distributions when the device has a poor CF less than 0.1, suggesting that the three channels are fully mixed. These channels will be gradually separated with the learning process. The second and third insets in Figure 2a show the light power distributions when the round of iteration reaches 50 and 85. The crosstalk becomes smaller gradually and the final crosstalk is below −16.8 dB at 1550 nm. Figure 2b shows the measured transmission spectra for different input-output optical routes. The crosstalk in the wavelength range of 1525−1575 nm is below −14 dB. In order to reveal the robustness of our self-configuring processor, we select another routing state of I_5-O_2, I_6-O_3, and I_7-O_1 as the training strategy, and the measured transmission spectra are shown in Figure 2c. The crosstalk values are lower than −23 dB at 1550 nm and lower than −13 dB in the wavelength range of 1525−1575 nm. These results demonstrate the reconfigurability and self-configuring ability of the chip for multichannel optical switching. More channels can be configured to switch if the network is further expanded.

https://dx.doi.org/10.1021/acsphotonics.9b01673
ACS Photonics 2020, 7, 792−799

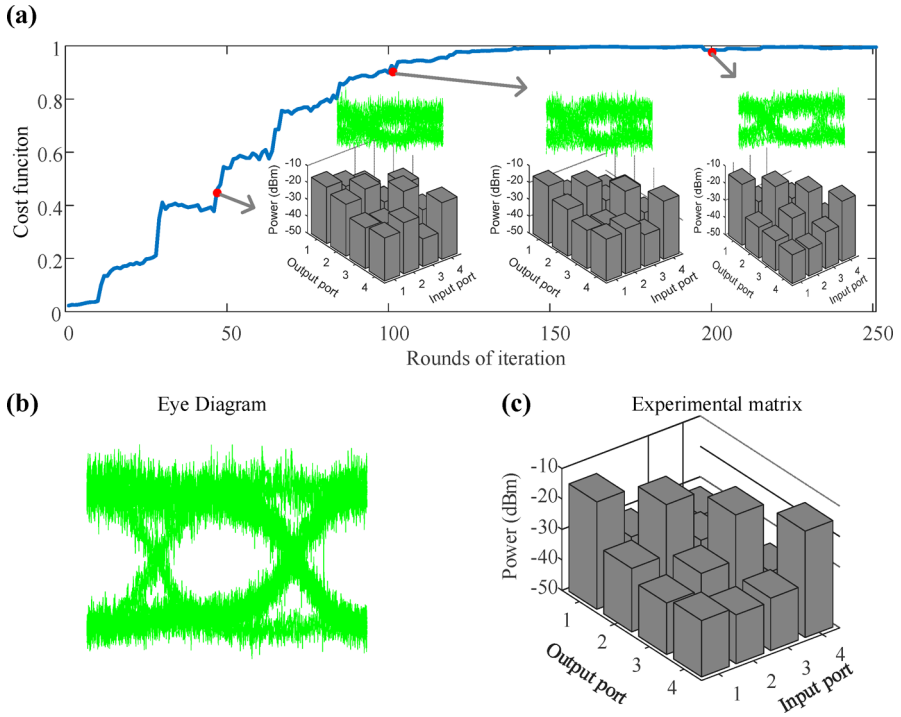

Figure 3. Optical MIMO descrambler. MZIs in Part (1) are used to switch the input channels, and the phase shifters in Part (2) are in random states to add crosstalk among these channels. The phase shifter built in the first MZI of Part (3) is set in the "open" state. All the other phase shifters in Parts (3) and (4) are used to optimize the performance at 1550 nm. (a) Cost function dependent on the rounds of iteration in training process. The insets figures show the eye diagrams of one monitored channel and light power distributions when the round of iteration equals 50, 100, and 200, respectively. (b) The final eye diagram of the monitored channel. (c) The final power distributions in the MIMO structure. Also see the Supporting Information of Video S2.

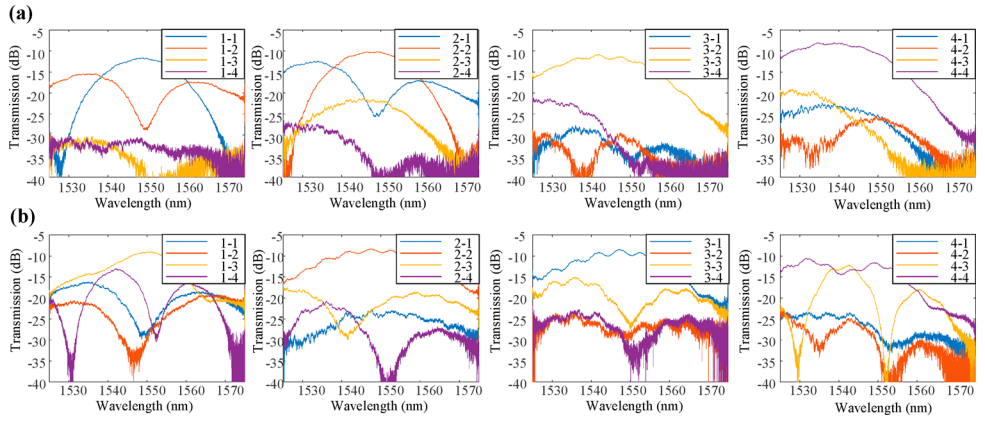

Figure 4. Transmission spectra for optical MIMO descrambler: (a) Routing state: I_1-O_1, I_2-O_2, I_3-O_3, I_4-O_4; (b) Routing state: I_1-O_3, I_2-O_2, I_3-O_1, I_4-O_4.

Optical MIMO Descrambler. The rapidly growing demand for higher transmission capacities promotes the development of MDM and SDM.[23,24] The crosstalk between different channels or modes always exists both in the optical transmission link and in the mode multiplexer/demultiplexer. Traditionally, this crosstalk issue was solved by MIMO algorithms in electronic digital signal processing,[51,52] which suffered from heavy computation requirements for high-bandwidth electronic hardware. Alternatively, all-optical MIMO demultiplexing was developed to descramble the modes with the inherent speed of light,[39,42,53] but these methods were based on manual operation or on the premise of knowing the internal structure of devices. Fortunately, gradient descent algorithm can be applied to MIMO descrambler as a fully self-configuring method. The MIMO descrambler is quite similar to the multichannel optical switching, except that the initial channels are already mixed owing to the crosstalk. In order to recover all channels with low crosstalk, the CF of MIMO descrambler is defined by eq 2, the same with the one of multichannel optical switching. In such a case, the targeted channels are well-defined before the crosstalk is introduced. In the experiment, Parts (1)−(4) are all enabled and the light is injected into input ports of I_1-I_4 and then output from O_1-O_4. Part (2) is used to emulate the optical transmission link and mode demultiplexer, where the crosstalk is accumulated by setting the voltages randomly, thus, introducing crosstalk among these channels coming from Part (1). Part (1) is used to switch the input channels. Parts (3) and (4) are used to

https://dx.doi.org/10.1021/acsphotonics.9b01673
ACS Photonics 2020, 7, 792−799

eliminate the crosstalk among these channels with the self-configuring algorithm.

Figure 3a presents the trainning process dependent on rounds of iteration in the routing state: I_1-O_1, I_2-O_2, I_3-O_3, I_4-O_4 (the iteration evolution is recorded by Video S2). Initially, the channel crosstalk is set randomly by applying random voltages on the phase shifters in Part (2), and then the network is trained by tuning the phase shifters in Parts (3) and (4) to make the CF maximal. Obviously, the crosstalk is quite strong before the training and the eye starts to open when the round of iteration equals to 50. As the iteration round increases, the CF grows and the crosstalk becomes smaller, which can be seen from the eye diagrams of the monitored channel (O_1) and light power distributions when the round of iteration equals to 100 and 200. Finally, the CF almost reaches the maximal theoretical value of 1. Figure 3b and c shows the final eye diagram of the monitored channel and light power distribution. The eye is fully open and the crosstalk is lower than −15 dB at 1550 nm. The transmission spectra for all channels are measured and presented in Figure 4a. The crosstalk is lower than −10 dB in a bandwidth of about 8 nm. Another routing state of I_1-O_3, I_2-O_2, I_3-O_1, I_4-O_4 is also demonstrated, the measured transmission spectra are shown in Figure 4b. The crosstalk values are lower than −12 dB at 1550 nm and lower than −10 dB in a bandwidth of about 5 nm. The narrow bandwidth results from the compromise on the small crosstalk, since the beams in each channel are from several paths with different optical lengths. Note that in the training process, the input channels are continuously switched and only one channel is switched on in each time. It means that the system cannot work during the training process.

In fact, once the MIMO descrambler successfully separates all channels after the training process, the CF can be redefined according to the signal quality of receiving channels. For example, we redefine the CF as the opening areas of eye diagrams of receiving channels by

$$\mathrm{CF} = \prod_{j=1}^{n} S\ \mathrm{area}_j \tag{3}$$

$S\ \mathrm{area}_j$ is the opening area of output eye diagram of Channel j. In such a case, the four channels can propagate real-time light signals during the training process. The training strategy is to make the opening areas of eye diagrams in the specified channels maximum. Restrained by the experimental conditions, we only train one channel to demonstrate this modified MIMO descrambler as a proof-of-concept. The evolution of eye diagram is shown in Figure 5 and recorded by Video S3, respectively. The opening area of the eye diagram in the specified channel gradually increases and becomes stable and maximal finally. If multiple channels need to train simultaneously, the CF can be set as the product of opening areas of eye diagrams in the targeted channels.

Tunable Optical Filter. Optical filter is a basic device in photonic signal processing. The reported tunable optical filters usually offer limited automaticity.[12,54] In our design, the cascaded MZI mesh shows great potential to adjust the transmission spectrum, acting as a smart tunable optical filter. In the experiment, we launch a broadband light source into the chip from input port I_4 and an OSA is used to monitor the output spectrum from output port O_4. The detailed experimental setup is presented in Figure S4 of Supporting Information, section 4. The CF is defined as the difference of average powers between the pass band and stop band, given by

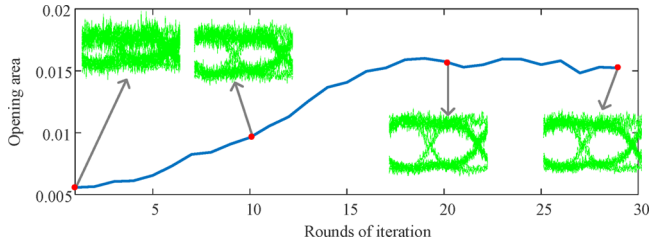

Figure 5. Modified MIMO descrambler when all four channels communicate normally. In the case, all the channels are open and working normally. Alternatively, the signal quality, such as the opening areas of eye diagrams, is used to offer the feedback information to optimize the performance. Also see the Supporting Information of Video S3.

$$\mathrm{CF} = \overline{P}_{\mathrm{pass}} - \overline{P}_{\mathrm{stop}} \tag{4}$$

where $\overline{P}_{\mathrm{pass}}$ is the average power in the pass band, and $\overline{P}_{\mathrm{stop}}$ is the average power in the stop band. All the phase shifters in Parts (2), (3), and (4) are jointly used to optimize the filter. Figure 6a presents the experimental results for tuning the central wavelength from 1537 to 1562 nm at a fixed full width at half-maximum (fwhm) of 20 nm. Figure 6b presents the measured spectra for bandwidth-tunable filter. The central wavelength is fixed at 1546 nm, and the fwhm is optimized from 18 to 32 nm. An example of filter evolution is shown by Video S4. The tunable range is mainly limited by the narrow-band coupling gratings (see Supporting Information, Figure S1b).

DISCUSSION AND SUMMARY

In our experiment, the voltage source is accessed by using serial port, so the communication speed is only about 10 Hz. The training is finished within 100 s (typically less than 1000 iterations), but the response speed of thermo-optic phase shifters is larger than 10 kHz.[55] The network training (typically less than 1000 iterations) can be completed within 100 ms, provided the external driver is fast enough. If the chip scale increases, the training time will increase correspondingly with the number of phase shifters. A faster training can be achieved using graphene microheater modulators,[56] free-carrier-depletion-based electro-optical modulators,[57] or hybrid silicon and lithium niobate modulators.[58]

The self-configuring method can effectively compensate the fabrication errors and avoid the clumsy manual operation. In fact, the multichannel optical switching can be further expanded to other routing networks with multiplexing technology, such as mode-division multiplexing (MDM), space-division multiplexing (SDM), wavelength-division multiplexing (WDM), and polarization-division multiplexing (PDM).[1,5] For example, the mixed channels distinguished by modes or polarization states can be initially separated and converted to the fundamental modes using the corresponding demultiplexer. Then our routing network is used to reconfigure the routing state using the self-configuring method. Finally, a mirrored multiplexer combines these separated channels by converting them to different modes or polarization states. Figure S3 (Supporting Information, section 4) depicts an example of mode switch with our multichannel optical switching device. Similar setup is applicable for SDM and

https://dx.doi.org/10.1021/acsphotonics.9b01673
ACS Photonics 2020, 7, 792−799

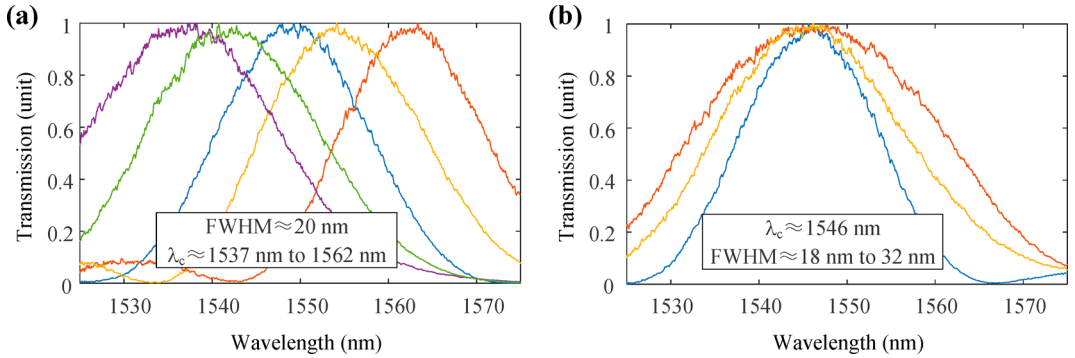

Figure 6. Tunable optical filter. A broadband light source is launched into the chip from I_4 and an optical spectrum analyzer is used to monitor the output spectrum from O_4, to optimize the filter. All the phase shifters in Parts (2), (3), and (4) are used. (a) Central wavelength adjustable filter. The full width at half-maximum (fwhm) is fixed at 20 nm, and the central wavelength is optimized from 1537 to 1562 nm. (b) Bandwidth adjustable filter. The central wavelength is fixed at 1546 nm, and the fwhm is optimized from 18 to 32 nm. Also see the Supporting Information of Video S4.

PDM channels as well. By combining the demultiplexer and multiplexer, our scheme can be configured for on-chip optical space, mode, wavelength, and polarization switching. The proposed two MIMO descramblers can be used in an optical network to perform fast signal processing without electronic digital sampling. They can be combined and applied in MDM-based optical communication. For example, the communication system can be initialized and calibrated using the first MIMO descrambler and then be optimized in real time using the modified MIMO descrambler. The modified MIMO descrambler can work without interrupting the communication, making the communication system has self-healing capabilities in real time. It is significant in optical communication. The tunable optical filter was also demonstrated, but the tunability is limited. It mainly comes from two aspects. On the one hand, the coupling gratings are narrowband with a 3 dB bandwidth about 40 nm (Supporting Information, Figure S1b), thus, restraining the tunable range. On the other hand, the MZIs are wavelength-insensitive in the waveband from 1525 to 1575 nm, making the tuning sensitivity quite low. A programmable optical filter, such as a shape-tunable filter, can be redesigned by a more wide-band coupling method, such as horizontal facet coupling, and by using a more wavelength-sensitive network, such as hexagonal cell structure and rectangular cell structure.[13,59]

In summary, we have designed, fabricated, and demonstrated a reconfigurable and fully self-configuring photonic integrated signal processor. The signal processor is reconfigured as a multichannel optical switching, two kinds of optical MIMO descramblers, and a tunable optical filter with a tunable central wavelength and a tunable bandwidth. All these functions are programmable by full self-configuration starting from blank. The training is accomplished using the numerical gradient descent algorithm modified from deep learning, which is applicable for a "black box" system. More complex and more accurate photonic signal processing functions can be accomplished using a larger network, such as an 8 × 8 network. Our demonstration is an important step toward the implementation of a multifunctional optical signal processor with the ability of programming and self-configuration.

■ ASSOCIATED CONTENT

Supporting Information

The Supporting Information is available free of charge at https://pubs.acs.org/doi/10.1021/acsphotonics.9b01673.

Sections 1−4 and Figures S1−S4 (PDF)
Video S1 (AVI)
Video S2 (AVI)
Video S3 (AVI)
Video S4 (AVI)

■ AUTHOR INFORMATION

Corresponding Author

Jianji Dong − *Wuhan National Laboratory for Optoelectronics, School of Optical and Electronic Information, Huazhong University of Science and Technology, Wuhan 430074, China;* orcid.org/0000-0002-1852-8650; Email: jjdong@hust.edu.cn

Authors

Hailong Zhou − *Wuhan National Laboratory for Optoelectronics, School of Optical and Electronic Information, Huazhong University of Science and Technology, Wuhan 430074, China; Photonics Research Centre, Department of Electronic and Information Engineering, The Hong Kong Polytechnic University, Hong Kong, China*

Yuhe Zhao − *Wuhan National Laboratory for Optoelectronics, School of Optical and Electronic Information, Huazhong University of Science and Technology, Wuhan 430074, China*

Xu Wang − *Wuhan National Laboratory for Optoelectronics, School of Optical and Electronic Information, Huazhong University of Science and Technology, Wuhan 430074, China*

Dingshan Gao − *Wuhan National Laboratory for Optoelectronics, School of Optical and Electronic Information, Huazhong University of Science and Technology, Wuhan 430074, China*

Xinliang Zhang − *Wuhan National Laboratory for Optoelectronics, School of Optical and Electronic Information, Huazhong University of Science and Technology, Wuhan 430074, China*

Complete contact information is available at: https://pubs.acs.org/10.1021/acsphotonics.9b01673

Author Contributions

[§]These authors contributed equally to this work.

https://dx.doi.org/10.1021/acsphotonics.9b01673
ACS Photonics 2020, 7, 792−799

Notes

The authors declare no competing financial interest.

■ ACKNOWLEDGMENTS

This work was partially supported by the National Key Research and Development Project of China (2018YFB2201901), the National Natural Science Foundation of China (61805090), the China Postdoctoral Science Foundation (2017M622419), the State Key Laboratory of Advanced Optical Communication Systems and Networks, Shanghai Jiao Tong University, China (2019GZKF03002), and the Hong Kong Scholars Program 2018 (XJ2018018).

■ REFERENCES

(1) Yang, L.; Zhou, T.; Jia, H.; Yang, S. L.; Ding, J. F.; Fu, X.; Zhang, L. General architectures for on-chip optical space and mode switching. *Optica* **2018**, *5* (2), 180−187.
(2) Sun, C. L.; Wu, W. H.; Yu, Y.; Chen, G. Y.; Zhang, X. L.; Chen, X.; Thomson, D. J.; Reed, G. T. De-multiplexing free on-chip low-loss multimode switch enabling reconfigurable inter-mode and inter-path routing. *Nanophotonics* **2018**, *7* (9), 1571−1580.
(3) Stern, B.; Zhu, X.; Chen, C. P.; Tzuang, L. D.; Cardenas, J.; Bergman, K.; Lipson, M. On-chip mode-division multiplexing switch. *Optica* **2015**, *2* (6), 530−535.
(4) Xiong, Y.; Priti, R. B.; Liboiron-Ladouceur, O. High-speed two-mode switch for mode-division multiplexing optical networks. *Optica* **2017**, *4* (9), 1098−1102.
(5) Zhang, Y.; He, Y.; Zhu, Q.; Qiu, C.; Su, Y. On-chip silicon photonic 2 × 2 mode- and polarization-selective switch with low inter-modal crosstalk. *Photonics Res.* **2017**, *5* (5), 521−526.
(6) Vlasov, Y.; Green, W. M. J.; Xia, F. High-throughput silicon nanophotonic wavelength-insensitive switch for on-chip optical networks. *Nat. Photonics* **2008**, *2* (4), 242−246.
(7) Spanke, R. A.; Benes, V. E. N-stage planar optical permutation network. *Appl. Opt.* **1987**, *26* (7), 1226−1229.
(8) Wang, J.; He, S. L.; Dai, D. X. On-chip silicon 8-channel hybrid (de) multiplexer enabling simultaneous mode-and polarization-division-multiplexing. *Laser Photon. Rev.* **2014**, *8* (2), L18−L22.
(9) Dai, D. X.; Li, C. L.; Wang, S. P.; Wu, H.; Shi, Y. C.; Wu, Z. H.; Gao, S. M.; Dai, T. G.; Yu, H.; Tsang, H. K. 10-Channel Mode (de)multiplexer with Dual Polarizations. *Laser Photon. Rev.* **2018**, *12* (1), 1700109.
(10) Wang, H. Y.; Dai, J. C.; Jia, H.; Shao, S. Z.; Fu, X.; Zhang, L.; Yang, L. Polarization-independent tunable optical filter with variable bandwidth based on silicon-on-insulator waveguides. *Nanophotonics* **2018**, *7* (8), 1469−1477.
(11) Magden, E. S.; Li, N.; Raval, M.; Poulton, C. V.; Ruocco, A.; Singh, N.; Vermeulen, D.; Ippen, E. P.; Kolodziejski, L. A.; Watts, M. R. Transmissive silicon photonic dichroic filters with spectrally selective waveguides. *Nat. Commun.* **2018**, *9* (1), 3009.
(12) Fandiño, J. S.; Muñoz, P.; Doménech, D.; Capmany, J. A monolithic integrated photonic microwave filter. *Nat. Photonics* **2017**, *11* (2), 124−129.
(13) Perez, D.; Gasulla, I.; Crudgington, L.; Thomson, D. J.; Khokhar, A. Z.; Li, K.; Cao, W.; Mashanovich, G. Z.; Capmany, J. Multipurpose silicon photonics signal processor core. *Nat. Commun.* **2017**, *8* (1), 636.
(14) Zhang, W.; Yao, J. A fully reconfigurable waveguide Bragg grating for programmable photonic signal processing. *Nat. Commun.* **2018**, *9* (1), 1396.
(15) Dai, D.; Liu, L.; Gao, S.; Xu, D. X.; He, S. Polarization management for silicon photonic integrated circuits. *Laser Photon. Rev.* **2013**, *7* (3), 303−328.
(16) Dai, D. X.; Bauters, J.; Bowers, J. E. Passive technologies for future large-scale photonic integrated circuits on silicon: polarization handling, light non-reciprocity and loss reduction. *Light: Sci. Appl.* **2012**, *1* (3), e1.
(17) Barwicz, T.; Watts, M. R.; Popović, M. A.; Rakich, P. T.; Socci, L.; Kärtner, F. X.; Ippen, E. P.; Smith, H. I. Polarization-transparent microphotonic devices in the strong confinement limit. *Nat. Photonics* **2007**, *1* (1), 57−60.
(18) Xu, H.; Shi, Y. Metamaterial-Based Maxwell's Fisheye Lens for Multimode Waveguide Crossing. *Laser Photon. Rev.* **2018**, *12* (10), 1800094.
(19) Li, S.; Zhou, Y.; Dong, J.; Zhang, X.; Cassan, E.; Hou, J.; Yang, C.; Chen, S.; Gao, D.; Chen, H. Universal multimode waveguide crossing based on transformation optics. *Optica* **2018**, *5* (12), 1549−1556.
(20) Dong, W.; Huang, Z.; Hou, J.; Santos, R.; Zhang, X. Integrated all-optical programmable logic array based on semiconductor optical amplifiers. *Opt. Lett.* **2018**, *43* (9), 2150−2153.
(21) Dong, J.; Zhang, X.; Wang, Y.; Xu, J.; Huang, D. 40 Gbit/s reconfigurable photonic logic gates based on various nonlinearities in single SOA. *Electron. Lett.* **2007**, *43* (16), 884.
(22) Yang, H.; Khayrudinov, V.; Dhaka, V.; Jiang, H.; Autere, A.; Lipsanen, H.; Sun, Z.; Jussila, H. Nanowire network-based multi-functional all-optical logic gates. *Sci. Adv.* **2018**, *4* (7), eaar7954.
(23) Richardson, D.; Fini, J.; Nelson, L. Space-division multiplexing in optical fibres. *Nat. Photonics* **2013**, *7* (5), 354−362.
(24) van Uden, R. G. H.; Correa, R. A.; Lopez, E. A.; Huijskens, F. M.; Xia, C.; Li, G.; Schülzgen, A.; de Waardt, H.; Koonen, A. M. J.; Okonkwo, C. M. Ultra-high-density spatial division multiplexing with a few-mode multicore fibre. *Nat. Photonics* **2014**, *8* (11), 865−870.
(25) Liu, W.; Li, M.; Guzzon, R. S.; Norberg, E. J.; Parker, J. S.; Lu, M.; Coldren, L. A.; Yao, J. A fully reconfigurable photonic integrated signal processor. *Nat. Photonics* **2016**, *10* (3), 190−195.
(26) Perez, D.; Gasulla, I.; Fraile, F. J.; Crudgington, L.; Thomson, D. J.; Khokhar, A. Z.; Li, K.; Cao, W.; Mashanovich, G. Z.; Capmany, J. Silicon Photonics Rectangular Universal Interferometer. *Laser Photon. Rev.* **2017**, *11* (6), 1700219.
(27) Perez, D.; Gasulla, I.; Capmany, J. Programmable multifunctional integrated nanophotonics. *Nanophotonics* **2018**, *7* (8), 1351−1371.
(28) Zhou, H. L.; Zhao, Y. H.; Wei, Y. X.; Li, F.; Dong, J. J.; Zhang, X. L. All-in-one silicon photonic polarization processor. *Nanophotonics* **2019**, *8* (12), 2257−2267.
(29) Zhou, H.; Zhao, Y.; Xu, G.; Wang, X.; Tan, Z.; Dong, J.; Zhang, X. Chip-Scale Optical Matrix Computation for PageRank Algorithm. *IEEE J. Sel. Top. Quantum Electron.* **2020**, *26* (2), 1−10.
(30) Zhao, Y.; Zhou, H.; Dong, J. An optical processor for matrix computation on Silicon-On-Insulator. *2019 24th OptoElectronics and Communications Conference (OECC) and 2019 International Conference on Photonics in Switching and Computing (PSC)*, IEEE, 2019, pp 1−3.
(31) Harris, N. C.; Steinbrecher, G. R.; Prabhu, M.; Lahini, Y.; Mower, J.; Bunandar, D.; Chen, C.; Wong, F. N. C.; Baehr-Jones, T.; Hochberg, M.; Lloyd, S.; Englund, D. Quantum transport simulations in a programmable nanophotonic processor. *Nat. Photonics* **2017**, *11* (7), 447−452.
(32) Tillmann, M.; Dakić, B.; Heilmann, R.; Nolte, S.; Szameit, A.; Walther, P. Experimental boson sampling. *Nat. Photonics* **2013**, *7* (7), 540−544.
(33) Shadbolt, P. J.; Verde, M. R.; Peruzzo, A.; Politi, A.; Laing, A.; Lobino, M.; Matthews, J. C. F.; Thompson, M. G.; O'Brien, J. L. Generating, manipulating and measuring entanglement and mixture with a reconfigurable photonic circuit. *Nat. Photonics* **2012**, *6* (1), 45−49.
(34) Wang, J.; Paesani, S.; Ding, Y.; Santagati, R.; Skrzypczyk, P.; Salavrakos, A.; Tura, J.; Augusiak, R.; Mancinska, L.; Bacco, D.; Bonneau, D.; Silverstone, J. W.; Gong, Q.; Acin, A.; Rottwitt, K.; Oxenlowe, L. K.; O'Brien, J. L.; Laing, A.; Thompson, M. G. Multidimensional quantum entanglement with large-scale integrated optics. *Science* **2018**, *360* (6386), 285−291.
(35) Qiang, X. G.; Zhou, X. Q.; Wang, J. W.; Wilkes, C. M.; Loke, T.; O'Gara, S.; Kling, L.; Marshall, G. D.; Santagati, R.; Ralph, T. C.; Wang, J. B. B.; O'Brien, J. L.; Thompson, M. G.; Matthews, J. C. F.

https://dx.doi.org/10.1021/acsphotonics.9b01673
ACS Photonics 2020, 7, 792−799

Large-scale silicon quantum photonics implementing arbitrary two-qubit processing. *Nat. Photonics* **2018**, *12* (9), 534−539.
(36) Carolan, J.; Harrold, C.; Sparrow, C.; Martin-Lopez, E.; Russell, N. J.; Silverstone, J. W.; Shadbolt, P. J.; Matsuda, N.; Oguma, M.; Itoh, M.; Marshall, G. D.; Thompson, M. G.; Matthews, J. C.; Hashimoto, T.; O'Brien, J. L.; Laing, A. QUANTUM OPTICS. Universal linear optics. *Science* **2015**, *349* (6249), 711−716.
(37) Harris, N. C.; Carolan, J.; Bunandar, D.; Prabhu, M.; Hochberg, M.; Baehr-Jones, T.; Fanto, M. L.; Smith, A. M.; Tison, C. C.; Alsing, P. M.; Englund, D. Linear programmable nanophotonic processors. *Optica* **2018**, *5* (12), 1623−1631.
(38) Mennea, P. L.; Clements, W. R.; Smith, D. H.; Gates, J. C.; Metcalf, B. J.; Bannerman, R. H. S.; Burgwal, R.; Renema, J. J.; Kolthammer, W. S.; Walmsley, I. A.; Smith, P. G. R. Modular linear optical circuits. *Optica* **2018**, *5* (9), 1087−1090.
(39) Annoni, A.; Guglielmi, E.; Carminati, M.; Ferrari, G.; Sampietro, M.; Miller, D. A. B.; Melloni, A.; Morichetti, F. Unscrambling light—automatically undoing strong mixing between modes. *Light: Sci. Appl.* **2017**, *6* (12), e17110.
(40) Miller, D. A. B. Self-configuring universal linear optical component [Invited]. *Photonics Res.* **2013**, *1* (1), 1−15.
(41) Ribeiro, A.; Ruocco, A.; Vanacker, L.; Bogaerts, W. Demonstration of a 4 × 4-port universal linear circuit. *Optica* **2016**, *3* (12), 1348−1357.
(42) Miller, D. A. Reconfigurable add-drop multiplexer for spatial modes. *Opt. Express* **2013**, *21* (17), 20220−20229.
(43) Clements, W. R.; Humphreys, P. C.; Metcalf, B. J.; Kolthammer, W. S.; Walsmley, I. A. Optimal design for universal multiport interferometers. *Optica* **2016**, *3* (12), 1460−1465.
(44) Shen, Y.; Harris, N. C.; Skirlo, S.; Prabhu, M.; Baehr-Jones, T.; Hochberg, M.; Sun, X.; Zhao, S.; Larochelle, H.; Englund, D.; Soljačić, M. Deep learning with coherent nanophotonic circuits. *Nat. Photonics* **2017**, *11* (7), 441−446.
(45) Lin, X.; Rivenson, Y.; Yardimci, N. T.; Veli, M.; Luo, Y.; Jarrahi, M.; Ozcan, A. All-optical machine learning using diffractive deep neural networks. *Science* **2018**, *361* (6406), 1004−1008.
(46) Reck, M.; Zeilinger, A.; Bernstein, H. J.; Bertani, P. Experimental realization of any discrete unitary operator. *Phys. Rev. Lett.* **1994**, *73* (1), 58−61.
(47) Hughes, T. W.; Minkov, M.; Shi, Y.; Fan, S. H. Training of photonic neural networks through in situ backpropagation and gradient measurement. *Optica* **2018**, *5* (7), 864−871.
(48) LeCun, Y.; Bengio, Y.; Hinton, G. Deep learning. *Nature* **2015**, *521* (7553), 436−444.
(49) Mnih, V.; Kavukcuoglu, K.; Silver, D.; Rusu, A. A.; Veness, J.; Bellemare, M. G.; Graves, A.; Riedmiller, M.; Fidjeland, A. K.; Ostrovski, G.; Petersen, S.; Beattie, C.; Sadik, A.; Antonoglou, I.; King, H.; Kumaran, D.; Wierstra, D.; Legg, S.; Hassabis, D. Human-level control through deep reinforcement learning. *Nature* **2015**, *518* (7540), 529−533.
(50) Silver, D.; Huang, A.; Maddison, C. J.; Guez, A.; Sifre, L.; van den Driessche, G.; Schrittwieser, J.; Antonoglou, I.; Panneershelvam, V.; Lanctot, M.; Dieleman, S.; Grewe, D.; Nham, J.; Kalchbrenner, N.; Sutskever, I.; Lillicrap, T.; Leach, M.; Kavukcuoglu, K.; Graepel, T.; Hassabis, D. Mastering the game of Go with deep neural networks and tree search. *Nature* **2016**, *529* (7587), 484−489.
(51) Arik, S. O.; Askarov, D.; Kahn, J. M. Effect of Mode Coupling on Signal Processing Complexity in Mode-Division Multiplexing. *J. Lightwave Technol.* **2013**, *31* (3), 423−431.
(52) Ryf, R.; Mestre, M. A.; Randel, S.; Schmidt, C.; Gnauck, A. H.; Essiambre, R. J.; Winzer, P. J.; Delbue, R.; Pupalaikis, P.; Sureka, A.; Sun, Y.; Jiang, X.; Peckham, D. W.; McCurdy, A.; Lingle, R. Mode-Multiplexed Transmission Over a 209-km DGD-Compensated Hybrid Few-Mode Fiber Span. *IEEE Photonics Technol. Lett.* **2012**, *24* (21), 1965−1968.
(53) Melati, D.; Alippi, A.; Melloni, A. Reconfigurable photonic integrated mode (de)multiplexer for SDM fiber transmission. *Opt. Express* **2016**, *24* (12), 12625−12634.
(54) Liao, S.; Ding, Y.; Peucheret, C.; Yang, T.; Dong, J.; Zhang, X. Integrated programmable photonic filter on the silicon-on-insulator platform. *Opt. Express* **2014**, *22* (26), 31993−31998.
(55) Zhou, H.; Yan, S.; Wei, Y.; Zhao, Y.; Cheng, Z.; Qie, J.; Dong, J.; Zhang, X. Silicon-based polarization analyzer by polarization-frequency mapping. *APL Photonics* **2018**, *3* (10), 106105.
(56) Yan, S.; Zhu, X.; Frandsen, L. H.; Xiao, S.; Mortensen, N. A.; Dong, J.; Ding, Y. Slow-light-enhanced energy efficiency for graphene microheaters on silicon photonic crystal waveguides. *Nat. Commun.* **2017**, *8*, 14411.
(57) Liu, K.; Ye, C. R.; Khan, S.; Sorger, V. J. Review and perspective on ultrafast wavelength-size electro-optic modulators. *Laser Photon. Rev.* **2015**, *9* (2), 172−194.
(58) He, M.; Xu, M.; Ren, Y.; Jian, J.; Ruan, Z.; Xu, Y.; Gao, S.; Sun, S.; Wen, X.; Zhou, L.; Liu, L.; Guo, C.; Chen, H.; Yu, S.; Liu, L.; Cai, X. High-performance hybrid silicon and lithium niobate Mach−Zehnder modulators for 100 Gbit s−1 and beyond. *Nat. Photonics* **2019**, *13* (5), 359−364.
(59) Zhuang, L. M.; Roeloffzen, C. G. H.; Hoekman, M.; Boller, K. J.; Lowery, A. J. Programmable photonic signal processor chip for radiofrequency applications. *Optica* **2015**, *2* (10), 854−859.

https://dx.doi.org/10.1021/acsphotonics.9b01673
ACS Photonics 2020, 7, 792−799